Identification of structures labeled by indocyanine green (ICG) in the rat choroid and retina can guide interpretation of ICG angiography

Dan Mejlachowicz, Patricia Lassiaz, Marta Zola, Bastien Leclercq, Emmanuelle Gélizé, Seiki Achiedo, Min Zhao, Antoine Rousseau, Francine Behar-Cohen

Article

Identification of structures labeled by indocyanine green (ICG) in the rat choroid and retina can guide interpretation of ICG angiography

Running title: What does ICG label

Dan Mejlachowicz[1], Patricia Lassiaz[1], Marta Zola[1,3], Bastien Leclercq[1], Emmanuelle Gélizé[1], Seiki Achiedo[1], Min Zhao[1], Antoine Rousseau[4], Francine Behar-Cohen[1,2,3,*]

[1] Centre de Recherche des Cordeliers, INSERM, Université Paris Cité, Sorbonne Université, Physiopathology of ocular diseases: Therapeutic innovations, Paris, France; mejlachowicz.dan@hotmail.fr; patricia.lassiaz@gmail.com; marta.zola9@gmail.com; baslecq@gmail.com; emmanuelle.gelize@gmail.com; seiki.achiedo@u-paris.fr; elodiecn@gmail.com

[2] Ophthalmopole Cochin University Hospital, Assistance Publique-Hôpitaux de Paris, France

[3] Department of ophthalmology, Hopital Foch, Suresnes, France

[4] Department of Ophthalmology, Bicêtre Hospital, Assistance Publique - Hôpitaux de Paris, Paris-Saclay University, French Reference Center for hereditary transthyretin amyloidosis (NNERF), French Reference Network for rare Ophthalmic diseases (OPHTARA), Le Kremlin-Bicêtre, France; arousseau1010@gmail.com

***** Correspondence: francine.behar@gmail.com

Abstract:

Purpose: Indocyanine green (ICG) is an albumin and lipoprotein binding dye absorbing in the far red used in angiography to visualize choroidal vessels (ICGA). To guide interpretation, ICG transport in the choroid, retinal pigment epithelial (RPE) and retina of rats was studied.

Methods: Two conditions were used: RPE/choroid organoculture (OC), incubated for 45 min in DMEM medium, 1% FBS containing 0.25 mg/ml ICG and RPE/choroid and neural retina flat-mounts at 1 and 6 hours after intravenous ICG injection (IV). Early and late sequences of ICGA were recorded until 6 hours. Ultra-deep red confocal microscope was used to localize ICG in flat-mounts and immunohistochemistry was performed for caveolin-1 (CAV1), tryptase (mast cell marker) and tubulin β3 (TUBB3)(nerve marker).

Results: In the OC, ICG penetrated homogeneously in the cytoplasm and stained the membranes of the RPE. At 1h after IV injection, ICG appeared in fine granules in RPE, partly labeled with CAV1 and decreasing at 6h. At 1h and 6h, ICG was found in the retinal vessels, faintly in the inner retina and in photoreceptor outer segments at 6 hrs. In the choroid, ICG co-localized with mast cells, immunostained with tryptase and accumulated along the large TUBB3-labeled nerve bundles. Hypothesis was raised on the interpretation of late ICGA infrared photography in case of transthyretin amyloidosis with neuropathy.

Conclusions: Beside being a vascular dye, ICG is transported from the vessels to the RPE towards the outer retina. It stains mast cells and large choroidal nerves. These observations could help the analysis of ICG-A images.

Keywords: indocyanine green; angiography; retina; choroid; choroidal nerve; mast cells; retinal pigment epithelium

Introduction

Indocyanine green angiography (ICGA) is used in clinical practice since more than 50 years, although its indication has decreased with the wide use of spectral domain optical coherence tomography (SD-OCT) and OCT angiography[1] since the main indication of ICGA is the visualization of choroidal neovascularization, often well identified by non-invasive imaging methods. Indeed, ICG is an amphiphilic, water soluble, tricarbocyanine dye with a molecular mass around 750 Da, that is >95% bound to HDL and LDL[2] (8) and to albumin after intravenous (IV) injection[3]. It is excited by wavelengths comprised between 750 and 800 nm and emits fluorescence that peaks at around 830 nm, avoiding interference with autofluorescence from surrounding tissues. Due to these chemical properties and its binding to plasma proteins and lipoproteins, ICG remains into normal choroidal vessels including the choriocapillaris and can be visualized through the pigmented retinal pigment epithelium, making it an ideal dye to image the choroidal vasculature with high contrast and sensitivity.

The clinical significance of ICGA is mostly based on the spatio-temporal localization of the fluorescence emitted by ICG after intravenous injection. The angiographic sequence allows to follow the very rapid filling of the arteries and choriocapillaris, followed by filling of the choroidal veins and drainage through the vorticose veins. Appearance of hyperfluorescence reflects leakage from choroidal vessels, whilst hypofluorescence indicates decreased perfusion or masking by absorbing structures but the kinetics of the hyper or hypofluorescence and their localization differs depending on the pathology and the disease mechanisms. We will not detail here the ICGA semiology that has been well reviewed by others who showed its value for diagnosis and even for prognosis in some chorioretinal diseases [1, 4-6]. When interpretating ICGA, beside its kinetics, several factors that influence ICG fluorescence should be considered, including its concentration and its binding to different surfaces. Particularly, the fluorescence intensity might increase at low ICG concentrations (1μM), but strikingly decrease at high concentrations (10μM)[6]. Binding to albumin with high affinity might also increases ICG fluorescence [7]. This property was used to detect proteins in capillary electrophoresis as ICG is only weakly fluorescent in dilute aqueous solution, but its near infrared fluorescence is highly enhanced when it binds to proteins and specifically albumin[8]. More recently, Jang et al used plasmon resonance and saturation binding assay to show that ICG fluorescence *in vivo* is higher for albumin-bound ICG (2.1-fold at 1h post-injection) [9].

Beside visualization of the choroidal vasculature, ICGA has the potential to provide additional indirect information on the metabolic capabilities of the retinal pigment epithelium (RPE) and on the intracellular trafficking of albumin and lipoproteins in endothelial and in RPE cells. Chang et al. demonstrated that ICG

is slowly internalized by RPE cells *in vivo* in the primate and *in vitro* in human RPE cells [11,12]. Various vesicular transports have been described in RPE cells for HDLs thar are internalized after binding to scavenger receptor class B type I (SR-BI), which is a mechanism to import xantophylls into the retina [13] and, for albumin and LDL through caveolin-mediated transcytosis since caveolin-1 is highly expressed in RPE cells[14]. The vesicular transports could explain the kinetics of ICG internalization in RPE cells [11,12]. In endothelial cells, HDL partially co-localized with LDL, albumin, and transferrin in intracellular vesicles[15] suggesting that ICG could also be internalized in endothelial cells through vesicular transporters. In other fields of medicine, ICG is used as an adjuvant to surgery to localize and preserve nerves and to perform lymphography [16,17] since ICG labels nerves[18], which network is very dense in the human choroid[19]. But whether ICG could label choroidal nerves in normal or pathologic conditions has not yet been questioned.

In summary, understanding the *in vivo* kinetics of ICG fluorescence requires to take into consideration the vascular and RPE macromolecular transport mechanisms and how they might be impaired in pathogenic conditions, and to take also into account the specificities of the dye, which fluorescence depends on its concentration, binding capacities and pH, that are all susceptible for changes in the different studied diseases.

A more extensive identification of the fate of injected ICG and its interaction with the retina and choroid could guide our interpretation of the clinical images. With this objective in mind, we performed experiments to analyze how ICG is distributed in the retina and choroid in rats, either after intravenous injection or after ex *vivo* organoculture.

Materials and Methods

Animals

Animals were kept in pathogen-free conditions with food, water and litter, and housed in a 12-hour/12-hour light/dark cycle. Sprague Dawley albinos male and female rats between 3 and 12 months-old were used (n=22). Albinos rats were used to allow a better visualization of choroidal immune-labeled structures.

Indocyanine green angiography

Rats were anesthetized by IP injection of 100 mg/kg of ketamine (Clorkétam 1000, Virbac France) and 4 mg/kg of Xylazine (Rompun 2%, Bayer Healthcare, Loos, France). After pupil dilation, Indocyanine green (ICG, 200µl, 2.5mg/ml INFRACYANINE®, SERB, Paris, France) was injected intravenously in the tail of rats. ICG angiography was performed using Heidelberg Retina Angiograph II (Heidelberg Engineering, Inc., Dossenheim, Germany) to image choroidal circulation and visualize ICG tissue staining. Pictures were recorded at 1-3 min, 10-15 min, 30 min, 1 hour and 6 hours. Rats were euthanized by Euthasol-VET (300 mg/kg, Dechra, Northwich, United-Kingdom) either at 1 hour (IV-1h, n=6) or 6 hours (IV-6h, n=4). After enucleation, eyes were fixed in 4% paraformaldehyde (PFA) for 15 min at room temperature. After washing with DPBS (ThermoFisherScientific, Illkirch-graffenstaden, France), eyes were dissected, the RPE-choroid-sclera complex and the neural retina were post-fixed with acetone at -20°C for 10 min and proceeded for flat-mounting.

Organoculture (OC) Rats (n=9, 18 eyes) were euthanized by Euthasol-VET. After enucleation and dissection of the anterior segment, the posterior segment of the eyeball including retina, choroid and sclera was incubated immediately for 45 min in DMEM medium (41965039, Thermo Fisher Scientific, Illkirch-graffenstaden, France) with 1% fetal bovine serum (10270106, Thermo Fisher Scientific) and 10% ICG (2,5mg/ml, INFRACYANINE®) at 37°C (5% CO2). After washing with DPBS, the neuroretina was removed. The RPE-choroid-sclera complex was fixed with 4% PFA, then post-fixed with acetone for 10 min at -20°, and proceeded for flat-mounting. We chose a 10-fold higher concentration for the ex vivo experiments as compared to the in vivo experiments, as this experiment was designed as a positive control for RPE internalization of ICG.

Flat mounting and immunofluorescence Four radical incisions were performed on the neuroretina and RPE-choroid-sclera complex. To observe ICG staining, tissues were directly flat-mounted with Dako Omnis Fluorescence Mounting Medium (Agilent, Les Ulis, France) and counter stained with DAPI (1:5000) for nuclei staining. Ultra-deep red confocal microscope (Leica LAS X software, STELLARIS 5, Leica Microsystems, Wetzlar, Germany) with an excitation wavelength at 700 nm was used to visualize and capture ICG

123 staining. The RPE-choroid-sclera complex from 3 control rats without ICG injection was used to check the
124 autofluorescence at this wavelength.

125 The RPE-choroid-sclera and neural retina were also used for immunohistochemistry. Tissues were
126 permeabilized with 0.01% triton X100 (Merck, Darmstadt, Germany) in DPBS, blocked with 10% normal
127 goat serum (G6767, Merck, Darmstadt, Germany) in DPBS, and then incubated with primary antibodies
128 (Table 1) at appropriate dilution for 7 days at 4°C under gentle agitation. After washing with 0.01% Triton
129 X100/DPBS, tissues were incubated with adequate secondary antibodies respectively: AlexaFluo® 488 goat
130 anti-rabbit IgG (1:500, Thermo Fisher Scientific) and AlexaFluo® 488 donkey anti-mouse IgG (1:500, Thermo
131 Fisher Scientific). The nuclei were counterstained with DAPI (1:5000). RPE-choroid-sclera and neuroretina
132 were flat-mounted with Dako Omnis Fluorescence Mounting Medium and observed with confocal micro-
133 scope. Negative controls omitting the primary antibody were tested according to the above protocol and did
134 not show non specific labelling at the level of the RPE or at the level of the choroid.

135 Table 1. List of primary antibodies

Target	Dilution	Supplier
Rabbit anti-Caveolin-1/CAV1	1:300	Abcam, Cambridge, U.K
Mouse anti-Tryptase	1:300	Santa Cruz Biotechnology, Heidelberg, Germany
Mouse anti-Tubulin β3/ TUBB3	1:500	Biolegend, San Diego, USA
Rabbit anti-Ionized calcium binding adapter molecule 1/ IBA1	1:300	Wako, Neuss, Germany

136 *Case report of amyloidosis*

137 A 52-year-old female with hereditary transthyretin amyloidosis (hTTRA) caused by the p.Val50Met vari-
138 ant, was referred for an ophthalmological assessment. She had undergone a liver transplant 16 years ago
139 and was experiencing severe sensorimotor and autonomic neuropathy. The patient had a history of amy-
140 loidosis affecting both eyes, including vitreous opacities and severe glaucoma which required two filtering
141 surgeries and phaco-vitrectomy in the left eye. Her best corrected visual acuity was 20/25 in the right eye
142 and 20/200 in the left eye, with intraocular pressure measured at 30mmHg in the right eye and 10mmHg in
143 the left eye. Biomicroscopic examination disclosed bilateral typical fringed pupils, along with deposits on
144 the anterior lens capsule in the right eye and a posterior chamber intraocular lens in the left eye. Fundus
145 examination revealed mild vitreous deposits in the right eye, a clear vitreous cavity with amyloid remnants

in the peripheral vitreous of the left eye (which had undergone vitrectomy), as well as bilateral diffuse vascular sheathing and excavated optic discs.

Results

ICG is internalized in RPE cells through vesicular transport

No fluorescent signal was observed when RPE/choroid flat mounts were excited at 700 nm showing no autofluorescence of the tissues at this wavelength (Figure 1A). This negative control was systematically analyzed in each experiment. The fluorescence of ICG allowed to observe it was internalized homogeneously into RPE cells and was also located at the cell membrane at one hour after posterior segment incubation in the medium containing ICG (0.25mg/ml of DMEM 1% FBS, final concentration) (Figure 1B). One hour after intravenous injection of ICG (0.5mg), fluorescent signal was located inside RPE cells, mostly concentrated into vesicles (Figure 1C, inset, arrows). At 6 hours after intravenous injection, intracellular ICG-labeled vesicles were still visible although at lower density (Figure 1D and E, inset, white arrows).

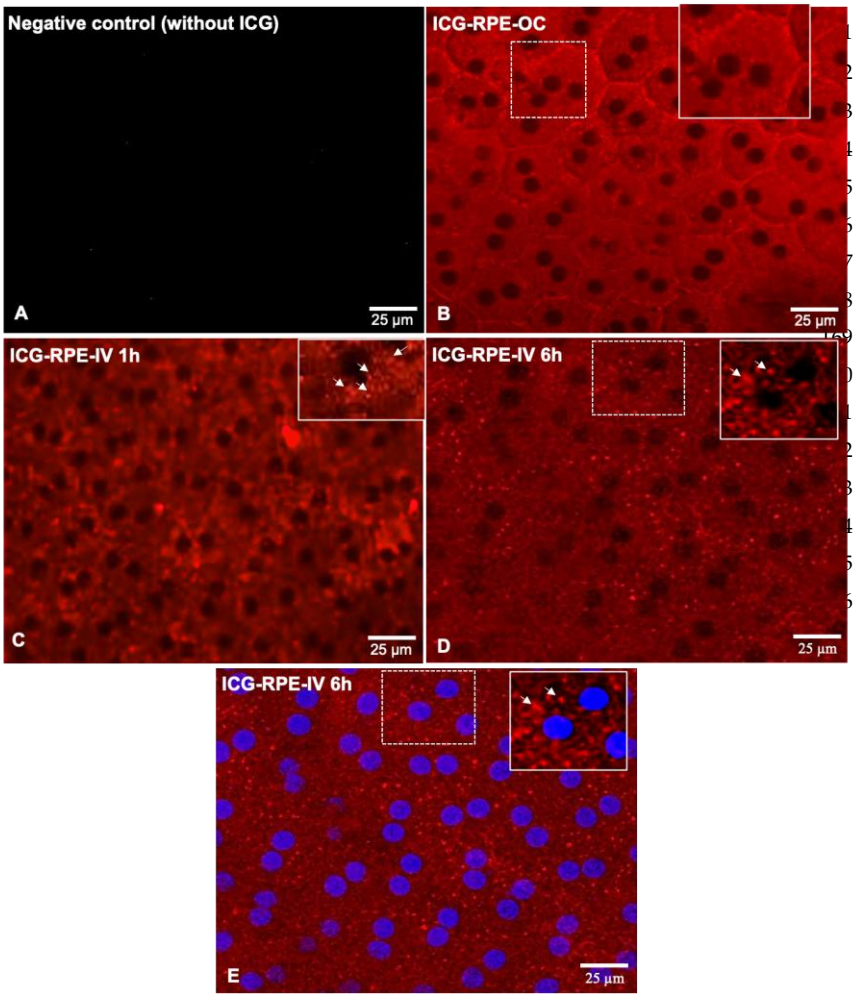

Figure 1

Deep infrared confocal imaging of retinal pigment epithelium (RPE)/ choroid flat mounts

A: No fluorescence when imaging is performed from the apical side without ICG.

B: 45 min after incubation in ICG, homogenous fluorescence of RPE cells and of their membranes (Inset).

C: One hour after ICG intravenous injection (IV), granular hyperfluorescence of RPE (inset).

D: Six hours after ICG IV, the granular hyperfluorescence decreases.

E: D image with nuclei DAPI staining.

Immunolocalization of caveolin-1 on RPE/choroid flat mounted at one hour after IV of ICG (Figure 2A and B), showed that at least part of the ICG-labelled intracellular vesicles were stained with caveolin-1 (Figure 2C, inset white arrows), demonstrating that ICG is partially transported in RPE through-caveola-mediated transcytosis. Specificity of the antibody is shown by the absence of staining on negative controls omitting the primary antibody (Figure 3A and D).

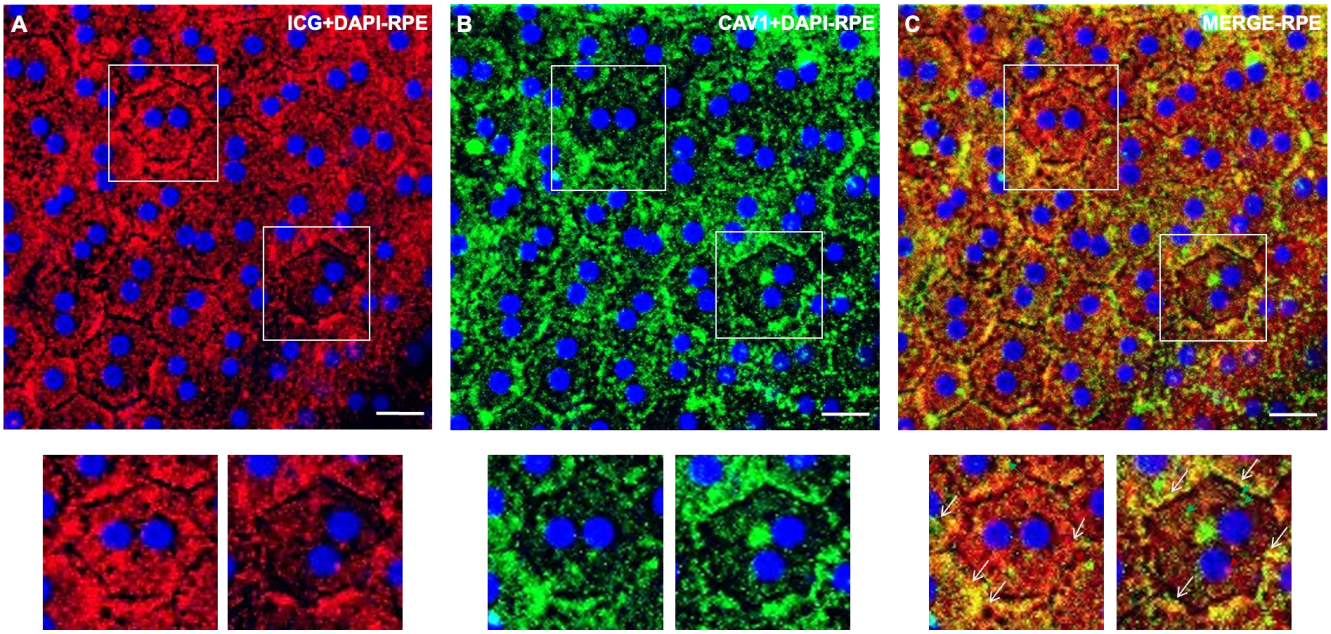

Figure 2

Deep infrared confocal imaging of RPE flat-mounts and caveolin-1 immunohistochemistry at one hour after IV injection of ICG

A: Deep infrared imaging of RPE showing granular staining with nuclei DAPI staining. Inset shows magnification. B: Caveolin-1 immunohistochemistry on RPE flat mount shows vesicular staining at the membrane and within the cytoplasm, with nuclei DAPI staining. Inset shows magnification. C: Merge of image A and B shows partial co-labelling of ICG with caveolin-1 with nuclei DAPI staining. Inset shows magnification with yellow co-stained vesicles (white arrows), caveolin-1 vesicles (green arrows) and ICG-stained vesicles (red arrows).

Scale bar: 20µm

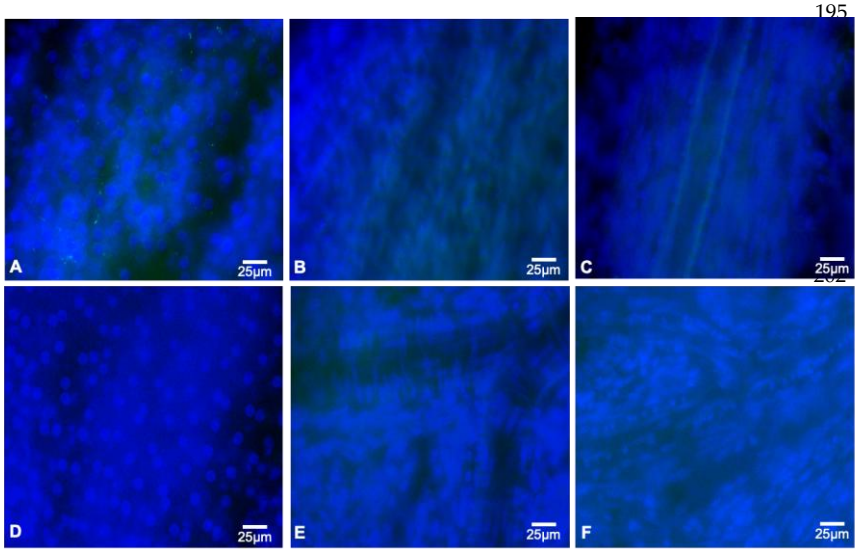

Figure 3

Negative controls without primary antibody in RPE/choroid flat mounts

A, D: AlexaFluo® 488 goat anti-rabbit in the RPE, negative control for Caveolin-1; B, E: AlexaFluo® 488 goat anti-rabbit in the choroid, negative control for IBA1; C, F: AlexaFluo® 488 donkey anti-mouse in the choroid,

negative control for Tryptase and TUBB3

ICG is transferred from choroid and RPE towards the outer retina

At one hour, ICG was still located in retinal vessels, probably inside endothelial cells, with faint ICG signal located around retinal vessels (Figure 4C and D), but no signal was observed either in the outer segments or in the outer plexiform layer (Figure 4A and B, and Figure 5). At 6 hours, ICG signal was present in the photoreceptor outer segments (Figure 4E, and Figure 5), with faint signal at the level of the outer plexiform layer, and decreased ICG signal in the retinal vessels (Figure 4G and H). Cross sections of the flat-mounted neural retina images confirmed the presence of ICG in the outer segments of the photoreceptors at 6 hours and increased staining from one to 6 hours in the ganglion cell layer (Figure 5 A and B). For a better visualization of ICG distribution in the retinal layers, videos of the full Z stacks confocal fluorescence imaging of neural retina flat mounts are available as Video 1 (1 hour) and 2 (6hours).

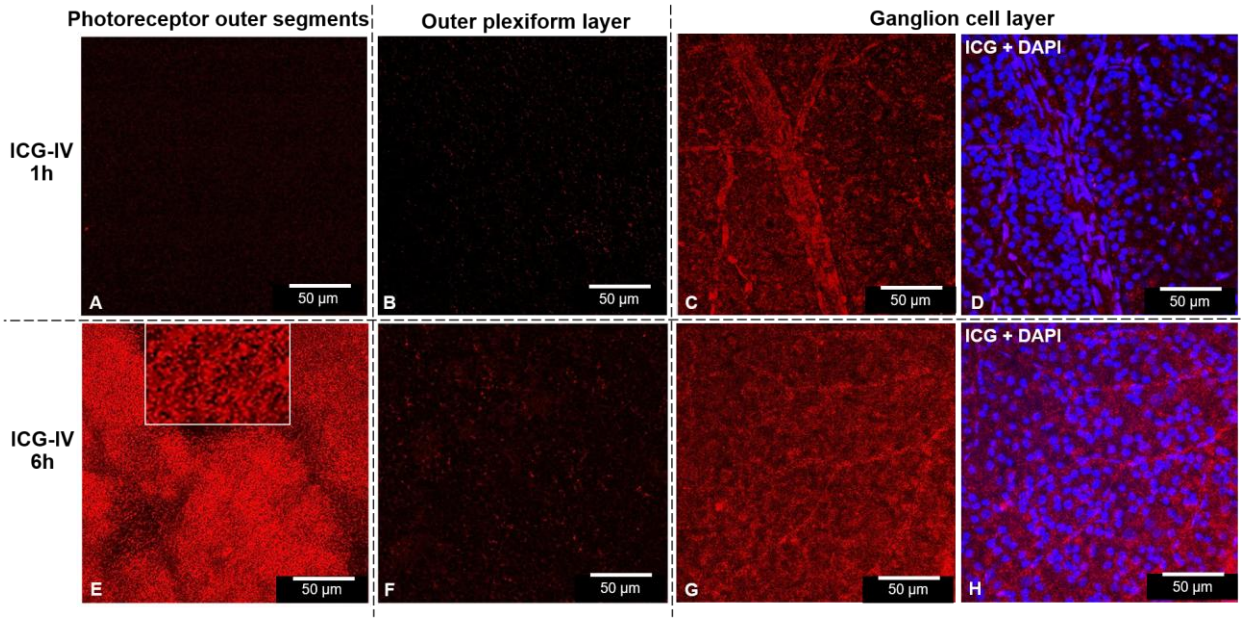

Figure 4

Deep infrared confocal imaging of neural retina flat mounts

A, B, C, D: one hour after ICG IV injection; outer segments (A), outer plexiform layer (B), ganglion cell layer (C), ganglion cell layer with DAPI nuclei staining (D).

E, F, G, H: six hours after ICG IV injection; outer segments (E), outer plexiform layer (F), ganglion cell layer (G), ganglion cell layer with DAPI nuclei staining (H).

Scale bar: 50µm

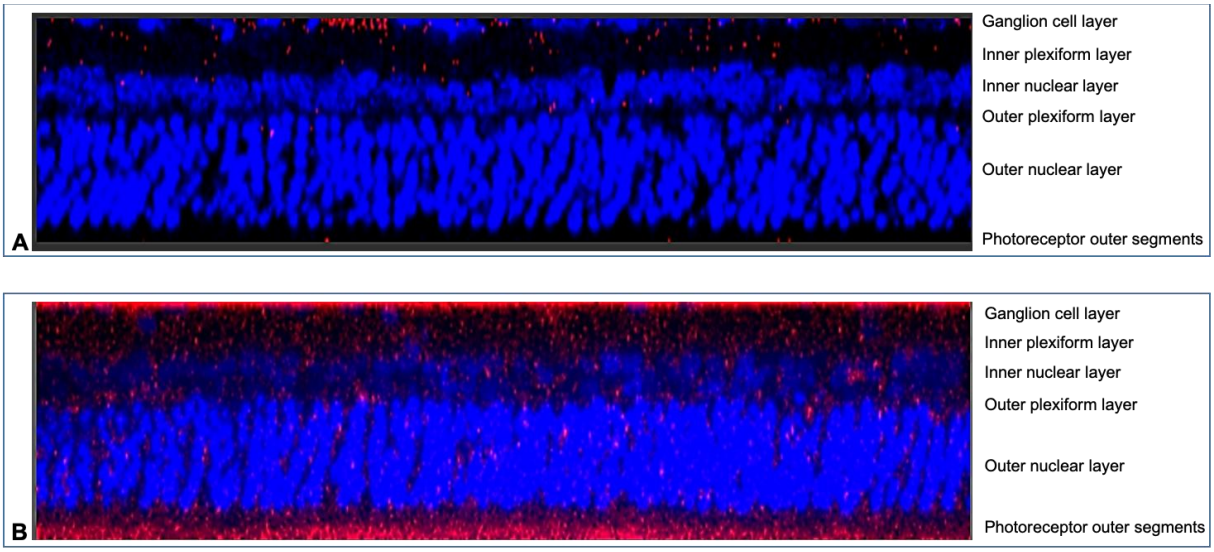

Figure 5

Cross sections of flat-mounted neural retina confocal images

Transverse pictures showing ICG with DAPI nuclei staining, from photoreceptor outer segments to the ganglion cell layer at 1hour (A) and 6hours (B) after ICG IV injection.

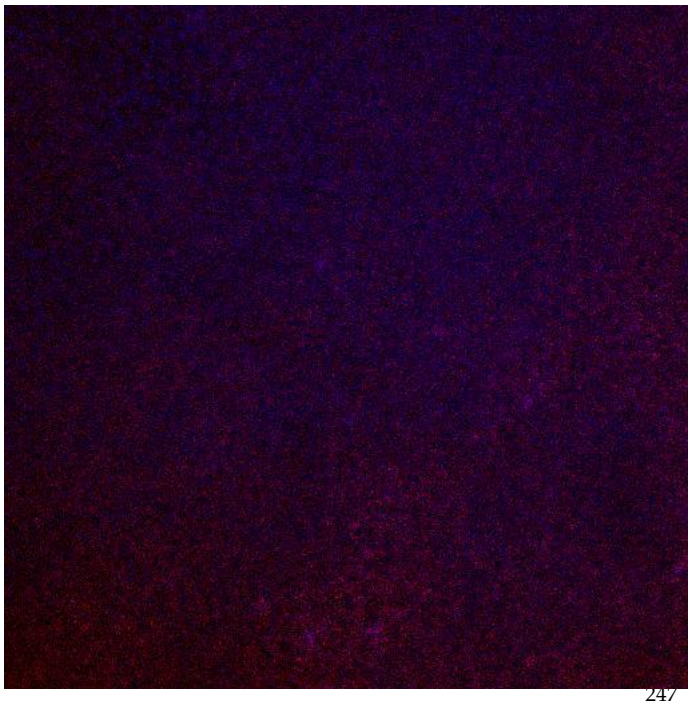

Video 1

Video of Z-stack confocal fluorescent images of neural retina flat mounts at one hour after ICG IV injectionICG with DAPI nuclei staining, from photoreceptor outer segments to the ganglion cell layer. Microscope: STELLARIS 5 (Leica Microsystems). Magnification: 40, distance: 73 μm, pixel size: 1 μm. Excitation wavelength: DAPI, 405 nm; ICG, 700 nm.

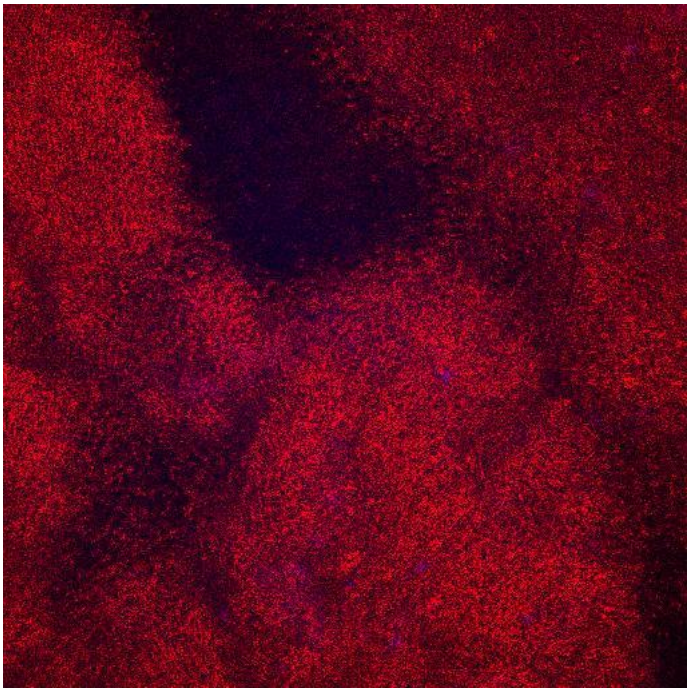

Video 2

Video of Z-stack confocal fluorescent images of neural retina flat mounts at six hour after ICG IV injectionICG with DAPI nuclei staining, from photoreceptor outer segments to the ganglion cell layer. Microscope: STELLARIS 5 (Leica Microsystems). Magnification: 40, distance: 78 µm, pixel size: 1 µm. Excitation wavelength: DAPI, 405 nm; ICG, 700 nm.

267

268 ***ICG stains mast cells and allows to identify large choroidal nerves***

269

270 When imaging the choroid from the scleral side, we could identify round large cells (15-30µm in diameter)
271 positively stained by ICG, aligned along the vessels, both after direct incubation of the posterior segment in
272 ICG and one hour after intravenous injection (Figure 6A and B). Higher magnification showed intracellular
273 granules positively stained with ICG (Figure 6C). Immunostaining with an antibody that recognizes
274 tryptase (a marker of at least part of the mast cells[20]) confirmed that those cells were mast cells (Figure 6D, E,
275 F) and not monocytic or dendritic cells, since they are not stained with ionized calcium-binding adapter
276 molecule 1 (IBA1) (Figure 6G). Negative controls are shown in Figure 3B and E for IBA1, and in Figure 3C
277 and F for tryptase.

278

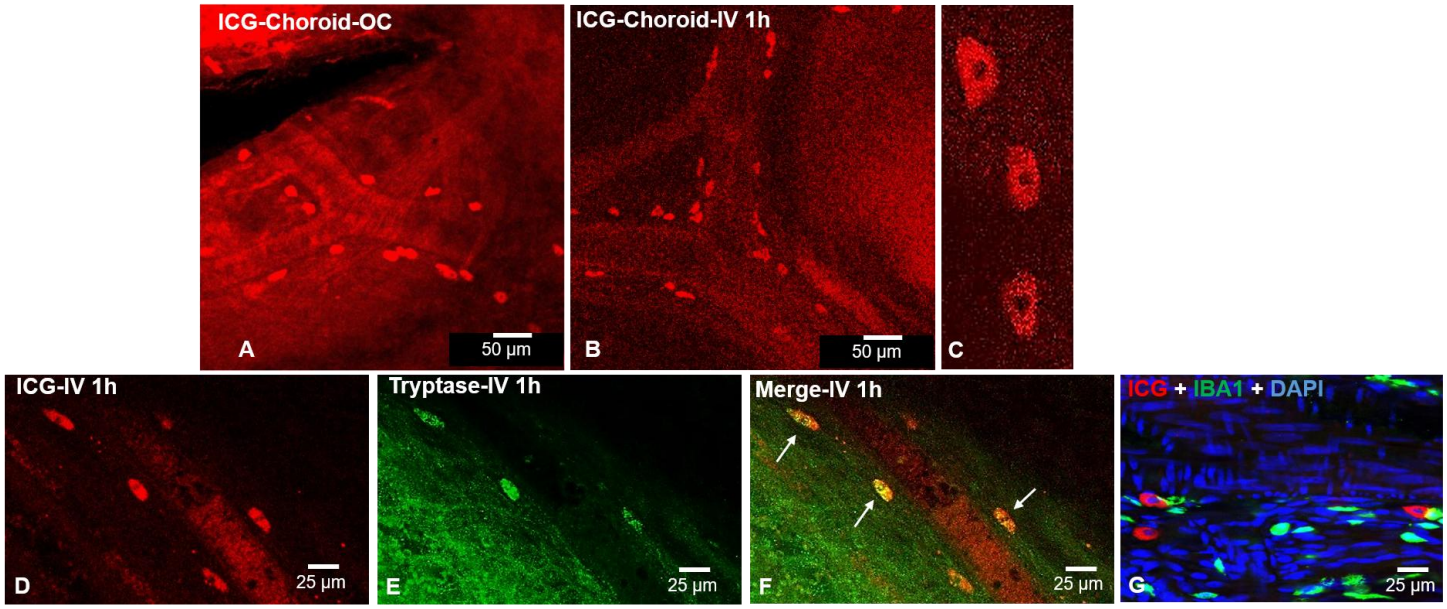

Figure 6

ICG staining of mast cells

A: ICG staining of perivascular cells 45 min after incubation of the RPE/choroid in ICG.
B-C: ICG staining of perivascular cells one hour after intravenous ICG injection with intracellular ICG positive granules (C). D, E, F: co-labeling of ICG-stained cells (D) with tryptase (E) showing co-labeled cells (F, arrows). G: Ionized calcium-binding adapter molecule 1 (IBA1) immunohistochemistry shows that ICG-positive cells are not labelled by IBA1.

The optic nerve head was only stained with ICG after incubation (Figure 7A) and not after IV. But, both after incubation and at one hour after IV of ICG, we identified filamentous ICG-positive bundles (Figure 7A and B) resembling choroidal nerves. Immunostaining with beta-tubulin 3 (TUBB3), a nerve marker [21] indicated that ICG binds the nerve bundle (Figure 7E, inset white arrows), whilst some nerve fibers seemed also stained with ICG (Figure 7H, inset dark star). Negative control for the antibody is shown in Figure 3 (C and F).

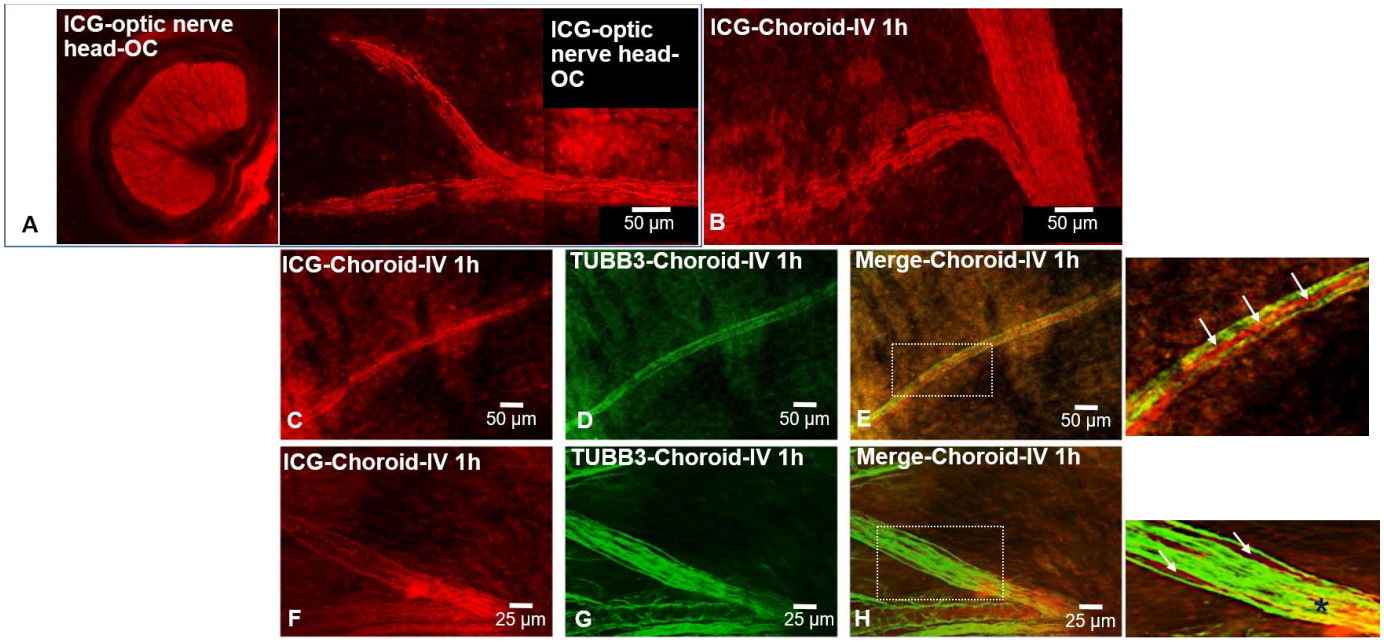

Figure 7

Large choroidal nerves identification by ICG

A: deep infrared of choroid flat-mount at 45 min after ICG incubation showing optic nerve head and large nerve. B, C and F: deep infrared of choroid at one hour after ICG intravenous injection showing that ICG-stains large nerves. D, G: Tubulin β3 (TUBB3) immunohistochemistry showing nerves fibers. E, H: co-staining of ICG with TUBB33 showing ICG around nerve fibers (E, inset white arrow).

Interpretation of ICGA in the rat

At the very early phase of ICGA (≤1min), the long ciliary posterior vessels (LCPV) emerging nearby the optic nerve are filled with ICG with a very rapid filling of the large veins, that can be followed in the mid periphery (Figure 8A, 30sec upper and lower images). Large retinal vessels are filled (Figure 9A) and vorticose veins (VV) are progressively visible (Figure 9A).

At 10 min, ICG can barely be detected in the long posterior ciliary vessels (LPCV) and in retinal vessels whilst a homogeneous background fluorescence can be detected with a hyperfluorescence around the optic nerve head (Figure 8B, upper image and Figure 9B). A closer analysis of the peripapillary fluorescence shows hyperfluorescent tracks along the vessels (Figure 9B, inset yellow arrows). At this time point, deep focalization probably shows bright fluorescence from the supra choroid and from the RPE. Along the LCPV at the periphery, a hyperfluorescent signal can be detected, and could correspond to branches of the ciliary nerves that travel along the vessels (Figure 8B and 9B, lower image yellow arrows).

At 1 hour, homogeneous background fluorescence is observed with dark vessels being visible underneath (Figure 8C). Higher magnification could detect possibly the RPE layer (Figure 8C, inset). There is still hyperfluorescence around the optic nerve and along the large ciliary vessels that could correspond to nearby nerves (Figure 8C, yellow arrow).

At 6 hours, the low hyperfluorescent background is still visible (Figure 9C) corresponding possibly to the RPE but also to the outer segments with still hyperfluoresence around the optic nerve head with tracks (Figure 8C, white arrows). Surrounding the choroidal vessels, hyperfluorescence could indicate choroidal nerves being labelled with ICG at this time point (Figure 9C, yellow arrows).

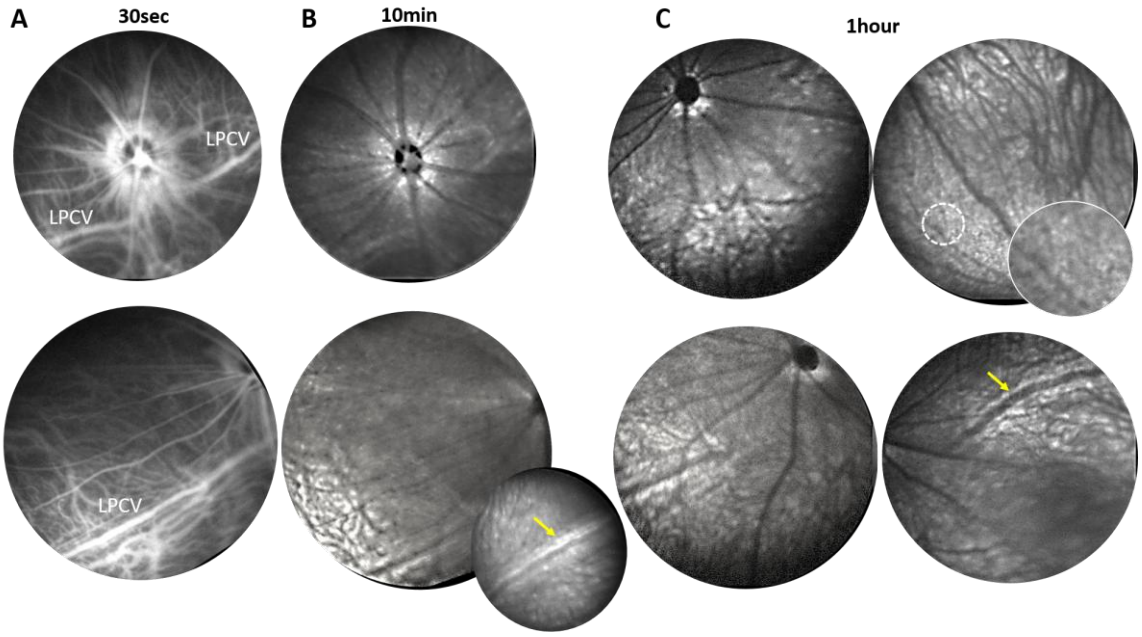

Figure 8

Indocyanine green angiography (ICGA) in albinos rats up to one hour

Indocyanine green angiography of Sprague Dawley albinos rats, showing early (30 sec) labelling of the long posterior ciliary vessels (LPCV) emerging at the posterior pole inferiorly to the optic nerve (A. upper image), and continuing towards the mid periphery (A. lower image). Optic nerve hyperfluorescence is seen in the very early phase with a peripapillary hyperfluorescent ring (A. upper image), whose intensity is attenuated, though still present, at 10 minutes and 1 hour (B. upper image and C. upper image, respectively). At 10mins, most of the retinal and choroidal vessels are visualized as hypofluorescent structures against a homogeneous hyperfluorescent background (B. upper and lower image). Along the hypofluorescent LPCV in the mid periphery, a linear hyperfluorescent signal can be observed (B. enlarged image, yellow arrow). One hour after ICG injection (C), the contrast between background fluorescence and vascular hypofluorescence becomes more evident. The granular background appearance in this late phase (C. upper right image and inset) could allow visualization of other, non-vascular components of the fundus. The mid-periphery pictures at 1h show that the hyperfluorescence along the LPCV is maintained (C. lower image left and right, yellow arrow).

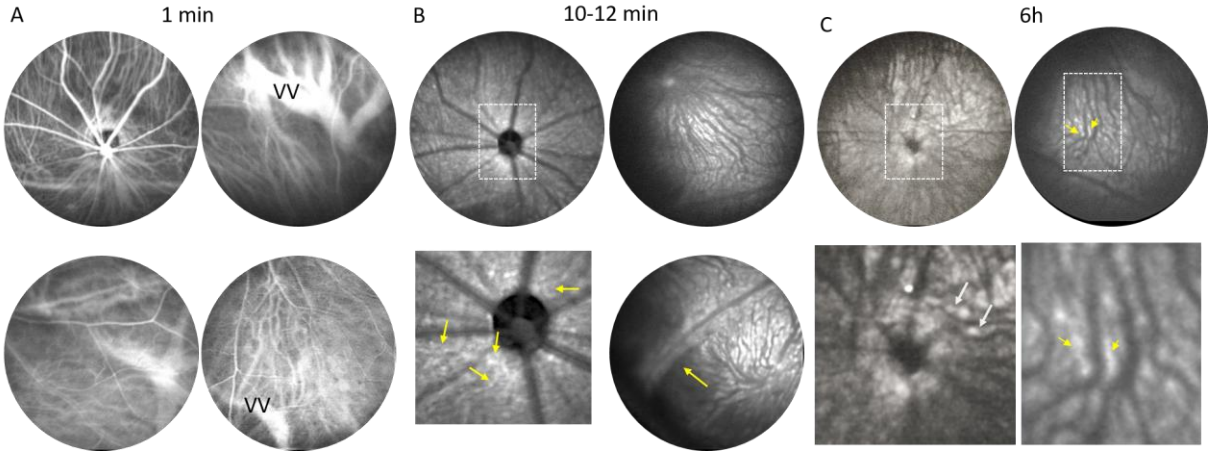

Figure 9

ICGA in albinos rats up to six hours

Indocyanine green angiography of Sprague Dawley albinos rats, showing early (1min) retinal and choroidal vascularization and venous drainage with vorticose veins (VV) progressively visible (A. all images). At 10 minutes, a closer analysis of the peripapillary hyperfluorescence shows linear hyperfluorescent structures (B. upper left image and lower enlarged left image, yellow arrows). The choroidal hypofluorescent vascular component is clearly visible against a hyperfluorescent background (B. upper right image). In the mid periphery, long posterior ciliary vessels are surrounded by a linear hyperfluorescence (B. lower right image). Six hours after ICG injection, a background fluorescence is detected underneath the dark retinal and choroidal vessels (C. upper left). The irregular peripapillary hyperfluorescence is showning detail (C. lower left image) where distinct hyperfluorescent structures are observed adjacent to vessels (white arrows). In the mid periphery (C. upper right image), irregular hyperfluorescence corresponds to linear perivascular structures (C. upper and lower right images, yellow arrows).

Interpretation of late phase ICGA in a case of amyloidosis

Amyloid deposits are visible on color fundus photographs as white-yellowish vascular sheathings (Figure 10A, white arrowheads, magnification in the dark circle) that are not labelled by ICG at any time point and particularly not at the late phase of the ICGA (Figure 10B and C). On the other hand, on the late ICGA image (>20min), typical ICG-positive elongated structures are visible in mid periphery and in the periphery of the fundus (Figure 10C), previously identified as vascular amyloid deposits in choroidal vessels, mostly arteries[22]. The reason why ICG would label the choroidal amyloid vascular deposits but not the retinal vessel amyloid deposits is unclear and we hypothesize that ICG could stain the pathological nerves of this patients presenting neuropathy. Superimposition of the late ICGA image with color fundus and comparison with the ICG stained vessels at the early ICGA phase, do not show clear co-localization between the elongated structures and the choroidal vessels (Figure 10, white circle on A, B, C), although small arteries could be hard to identify. The B-scan OCT, at the cross section with one of the elongated ICG positive structure shows

that the ICG-positive structure localizes with a round structure at the vicinity of a large choroidal vein, that does not contain the hyporeflective inside as observed in vessels.

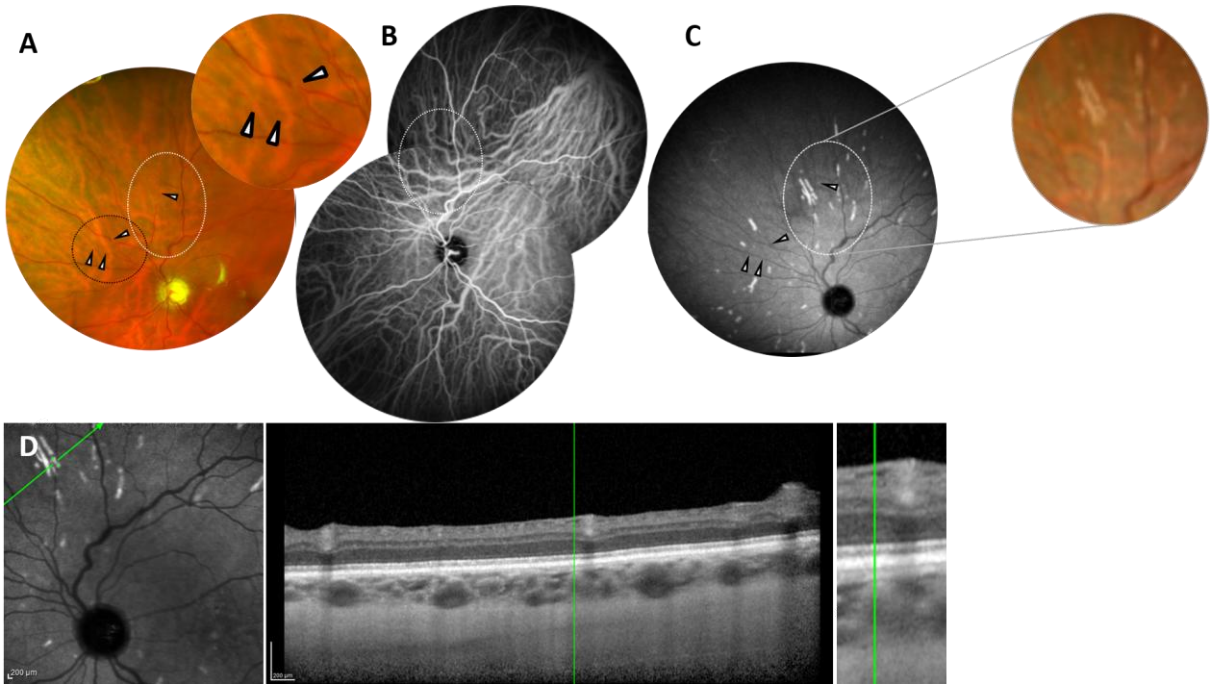

Figure 10

Retina images of a 52-year old female with hTTRA and amyloid neuropathy

A: color fundus showing white yellowish vascular sheathings observed along retinal vessels (white arrowheads, dark cercle with magnification). B: 2 min ICGA infrared photography .C: 27 min ICGA infrared photography, showing no staining of the amyloid deposits in retinal vessels (white arrowheads) and the ICG stained elongated dots and tracks. White circle in A, B, and C corresponds to the same area with superimposition of C and D on the magnified image in C. D: B-scan along the ICGA stained elongated structures with the green line indicating the cross section with one of them. Magnification shows that it does not correspond to the typical image of a choroidal vessel.

Discussion

We have used albinos rats to follow the fate of ICG after either IV injection or direct incubation of the ocular tissues from the posterior segment of the eye in ICG and we have imaged the fluorescence ocular tissues at late time points as compared to the classical angiographic sequence. The idea behind this experimental setting was to help understand clinical images taken at the late phases of the angiographic sequence, considering that the direct observation of ICG using confocal microscopy on flat-mounted tissues is much more sensitive than in vivo angiography. Indeed, the late phase of ICGA remains difficult to interpret in several clinical conditions. We recently analyzed the mid-phase hyperfluorescent plaques

(6-10min) observed on ICGA in patients with central serous chorioretinopathy (CSCR) and discussed the reason for the complete fading of fluorescence at later time point (>20min), which differs from the hyperfluorescence linked to type 1 macular neovascularization in AMD that remains fluorescent on the late phases [23,24]. The reason for the intriguing ICG kinetics in multiple evanescent white dot syndrome was questioned recently by Gaudric and Mrejen[25].

The choice for albinos rat was made to allow immunolocalization of various structures together with ICG imaging, whilst reducing the absorption due to melanin. Interpretation of our observation must thus consider this important difference with the pigmented human RPE/choroid. The use of a confocal microscope with simultaneous lines from 405 to 685nm and detectors on three spectral channels provided high photon detection efficiency and extremely low dark noise as well as extended detection into the near infrared of up to 850 nm. In addition, we could overlap infrared imaging and other fluorophores to perform immunolocalization.

As previously described by several authors, we observed that either after ICG intravenous injection or after incubation of ocular tissues at 37°C, ICG-bound molecules were internalized into the RPE cells, although ICG accumulated also at the cell membrane after incubation and not after IV injection. After intravenous injection in non-human primate, Chang et al showed that ICG was internalized within 15 to 50 minutes with increasing fluorescent signal in the RPE cells at the later time points[10]. Several studies were also performed in rodents showing not only that ICG was internalized by RPE cells after IV injection, but that it remained detectable for an extended period of time and up to 28 days, particularly when high dose of ICG (5mg/kg) was injected[26]. In our experiments, we used 1.5-2mg/kg which corresponds to high ICG dose, explaining that the ICG staining remained at 6 hours. The precise localization of ICG showed that at least part of it, is transported in vesicles that were positively labeled with caveolin-1 antibodies, suggesting that caveolae-mediated transcytosis is involved in ICG transport, which is a well down mechanism for albumin transport within cells[26] and a mechanism for albumin transcytosis in endothelial microvascular cells [27]. Transcytosis of LDL is also regulated by caveolin 1-mediated mechanisms in endothelial cells[28]. In the retina, caveolin-1 is expressed in retinal vascular cells, Müller glial cells and RPE cells[29], but the exact role of caveolin-1 in the protein and lipoprotein transports between the choroidal circulation and the neural retina is not yet fully understood. Lipoproteins, to which ICG is highly bound, are also transported from the choroidal blood flow towards the RPE and are responsible for the delivery of vitamin A, carotenoids and of lutein and zeaxanthin towards the inner retinal layers in the macula through the RPE [30], demonstrating that transcytosis can occur also to allow the exit of molecules at the apical side of the RPE. Tserentsoodol et al

showed that after intravenous injection of fluorescently labeled LDL and HDL, fluorescent signal was observed in the choriocapillaris, the RPE and part of the neural retina at 2 hours, and that signal was detected in the outer segment of photoreceptors at 4 hours[31], which is consistent with our observation of ICG signal in the outer segments at 6 hours and not at one hour after IV injection. Altogether, in the rat retina, the fate of intravenously injected ICG, which binds to lipoproteins and to albumin, reflects well the known kinetics of albumin and lipoprotein transports into the retina.

The reason for ICG accumulation in mast cells can be understood by the fact that mast cells metabolize lipoproteins and rapidly internalizes LDL [32], particularly when activated[33]. Since not all mast cells were tryptase positive and not all tryptase positive cells were ICG-labeled, it cannot be excluded that several types of mast cells with various activation states are present in the choroid. Mast cells, enriched along large vessels in the choroid play important role in physiopathology and can induce subretinal fluid accumulation and inflammation upon degranulation[34]. ICG-A should be re-analyzed in cases of choroidal inflammation with a specific focus on hyperfluorescent dots with the idea that such dots (around 50µm) could represent activated mast cells.

Finally, we have identified that ICG accumulates in choroidal nerves, particularly the large bundles, which reflects well the known entry of albumin into the endoneurial space through the endoneurial vasculature at 1.2 mg.g-1.day-1 and with a daily turnover of endoneurial albumin of about 30% [35]. Mata et al showed that serum albumin is found within the perineurium and endoneurium but not in the axon, suggesting that axons are exposed to serum proteins in normal nerves[36]. The late phase ICGA hyperfluorescent dots and tracks found in the retinal periphery of eyes with transthyretin amyloidosis angiopathy[21] might correspond, at least in part, to large choroidal nerves running in the walls of choroidal vessels, mostly arteries, and not to vascular amyloid plaques since plaques in retinal vessels, clearly observed on the fundus photography are not stained by ICG at all the angiographic times of the sequence (Figure 8). If such amyloid deposits were stained by ICG, retinal plaques should also be stained as intramural deposits alter the endothelial integrity giving access to ICG [37]. In addition, amyloid neuropathy, particularly alteration of nerves from the autonomous nervous system is part of the clinical signs of the disease[38] and increase of albumin entry in the endoneurium through endothelial alterations is an indicator of pathologic nerves[37–39]. ICG angiography is

not commonly performed in patients with diabetic retinopathy, although it has been used to identify the early occurrence of choroidal pathology[40]. Since diabetic patients with retinopathy often suffer from peripheral neuropathy, including autonomic neuropathy[41], late phase ICG might be useful to reveal choroidal neuropathy in diabetic eyes.

The interpretation of clinical ICG angiography images from observations made on albinos rats is far from being straightforward, partly because these are albinos animals and partly because the observation times are longer than those usually used in the clinical examinations. However, the numerous hyper or hypofluorescent ICG images that we observe but whose significance we do not fully understand should be analyzed with a new perspective considering that ICG is a unique tool to follow the metabolism of proteins and lipoproteins in the eye and not only an inert dye. ICGA image interpretation should also consider that the fluorescence properties of ICG depend on the concentration of ICG when bound to proteins and that high local concentrations can induce hypofluorescence by quenching mechanisms.

The observation we report herein open new perspectives in the use of ICG as a metabolic marker but also a marker of the neural and immune components of the choroid. If ICG-angiography could improve the identification of choroidal neuropathy in several retinal disease, it could help our understanding of disease and their treatments.

Similar studies should be replicated in non-human primates for better translation to the clinic.

Funding: This research was funded by the Agence Nationale de la Recherche (ANR-20-CE17-0034). We thank The Abraham J. & Phyllis Katz Foundation for their financial support for conducting research.

Institutional Review Board Statement: The animal study protocol was performed in accordance with the European Communities Council Directive 86/609/EEC and French national regulations and approved by local ethical committees (#25158, Charles Darwin).

Data Availability Statement: The data from the study are available from the corresponding author upon reasonable request.

Acknowledgments: The authors acknowledge Theano Irinopoulou at the imaging platform of Fer à Moulin Institute (Paris, France) for its technical support.

Conflicts of Interest: The authors declare no conflict of interest.

References

1. S. Y. Cohen, L. Dubois, G. Quentel, A. Gaudric, Is indocyanine green angiography still relevant? 2011; *Retina*. **31**, 209–221.
2. S. Yoneya, T. Saito, Y. Komatsu, I. Koyama, K. Takahashi, J. Duvoll-Young, Binding properties of indocyanine green in human blood. *Invest Ophthalmol Vis Sci*. 1998; **39**, 1286–1290.
3. E. D. Moody, P. J. Viskari, C. L. Colyer, Non-covalent labeling of human serum albumin with indocyanine green: a study by capillary electrophoresis with diode laser-induced fluorescence detection. *J Chromatogr B Biomed Sci Appl*. 1999; **729**, 55–64
4. K. D. Kovacs, B. Young, R. A. Adelman, Quantitative Modeling of Ultra-Widefield Choroidal Indocyanine Green Angiography in Systemic Vascular Diseases. *Ophthalmic Surg Lasers Imaging Retina*. 2021; **52**, 281–287.
5. S. Borooah, P. Y. Sim, S. Phatak, G. Moraes, C. Y. Wu, C. M. G. Cheung, B. Pal, D. Bujarborua, Pachychoroid spectrum disease. *Acta Ophthalmol* 2020, doi:10.1111/aos.14683.
6. C. M. G. Cheung, M. Y. Z. Wong, K. Y. C. Teo, CHOROIDAL VASCULAR ALTERATIONS IN AGE-RELATED MACULAR DEGENERATION AND POLYPOIDAL CHOROIDAL VASCULOPATHY. *Retina*. 2023; **43**, 1–7 .
7. M. Nairat, A. Konar, M. Kaniecki, V. V. Lozovoy, M. Dantus, Investigating the role of human serum albumin protein pocket on the excited state dynamics of indocyanine green using shaped femtosecond laser pulses. *Phys Chem Chem Phys*. 2015; **17**, 5872–5877.
8. R. Mačianskienė, M. Almanaitytė, R. Treinys, A. Navalinskas, R. Benetis, J. Jurevičius, Spectral characteristics of voltage-sensitive indocyanine green fluorescence in the heart. Sci Rep 2017; Aug 11;7(1):7983
9. H. J. Jang, M. G. Song, C. R. Park, H. Youn, Y.-S. Lee, G. J. Cheon, K. W. Kang, Imaging of Indocyanine Green-Human Serum Albumin (ICG-HSA) Complex in Secreted Protein Acidic and Rich in Cysteine (SPARC)-Expressing Glioblastoma. *Int J Mol Sci*. 2023; **24**, 850.
10. L. Chen, P. Yang, C. A. Curcio, Visualizing lipid behind the retina in aging and age-related macular degeneration, via indocyanine green angiography (ASHS-LIA). *Eye (Lond)* 2022*;* . **36**, 1735–1746.
11. A. A. Chang, L. S. Morse, J. T. Handa, R. B. Morales, R. Tucker, L. Hjelmeland, L. A. Yannuzzi, Histologic localization of indocyanine green dye in aging primate and human ocular tissues with clinical angiographic correlation. *Ophthalmology*. 1998; **105**, 1060–1068 .
12. A. A. Chang, M. Zhu, F. Billson, The interaction of indocyanine green with human retinal pigment epithelium. *Invest. Ophthalmol. Vis. Sci.* 2055; **46**, 1463–1467.
13. S. E. Thomas, E. H. Harrison, Mechanisms of selective delivery of xanthophylls to retinal pigment epithelial cells by human lipoproteins. *J Lipid Res*. 2016; **57**, 1865–1878 .
14. E. N. Enyong, J. M. Gurley, M. L. De Ieso, W. D. Stamer, M. H. Elliott, Caveolar and non-Caveolar Caveolin-1 in ocular homeostasis and disease. *Prog Retin Eye Res*. 2022; **91**, 101094.

15. D. Perisa, L. Rohrer, A. Kaech, A. von Eckardstein, Itinerary of high density lipoproteins in endothelial cells. *Biochim Biophys Acta*. 2016; **1861**, 98–107.
16. N. Amara, T. Al Youssef, J. Massa, A. Fidjel, E. E. Khoury, B. Patel, M. Flais, C. Deswarte, Intraoperative angiography of the neurovascular bundle using indocyanine green and near-infrared fluorescence improves anatomical dissection during robot-assisted radical prostatectomy: initial clinical experience. *J Robot Surg*. 2023; **17**, 687–694.
17. Patel V, Kulich M, Kochhar A, Gomez G.Endoscopic-Indocyanine Green Angiography Assisted Microtia Reconstruction. Laryngoscope. 2023 Dec;133(12):3615-3618.
18. T. Géczi, Z. Simonka, J. Lantos, M. Wetzel, Z. Szabó, G. Lázár, J. Furák, Near-infrared fluorescence guided surgery: State of the evidence from a health technology assessment perspective. *Front Surg*; 2022. **9**, 919739
19. Leclercq B, Weiner A, Zola M, Mejlacowicz D, Lassiaz P, Jonet L, Gélizé E, Perrot J, Viengchareun S, Zhao M, Behar-Cohen F.The choroidal nervous system: a link between mineralocorticoid receptor and pachychoroid. Acta Neuropathol. 2023 Nov;146(5):747-766.
20. D. Atiakshin, I. Buchwalow, M. Tiemann, Mast cell chymase: morphofunctional characteristics. *Histochem. Cell Biol.* 2019; **152**, 253–269.
21. M. K. Fath, F. Zahedi, Z. S. Hashemi, S. Khalili, Evaluation of Differentiation Quality of Several Differentiation Inducers of Bone Marrow-derived Mesenchymal Stem Cells to Nerve Cells by Assessing Expression of Beta-tubulin 3 Marker: A Systematic Review. *Curr Stem Cell Res Ther*. 2021; **16**, 994–1004.
22. A. Rousseau, C. Terrada, S. Touhami, E. Barreau, P.-R. Rothschild, S. Valleix, F. Benoudiba, M.-H. Errera, C. Cauquil, A. Guiochon-Mantel, D. Adams, M. Labetoulle, Angiographic Signatures of the Predominant Form of Familial Transthyretin Amyloidosis (Val30Met Mutation). *Am J Ophthalmol*. 2018; **192**, 169–177.
23. E. Bousquet, J. Provost, M. Zola, R. F. Spaide, C. Mehanna, F. Behar-Cohen, Mid-Phase Hyperfluorescent Plaques Seen on Indocyanine Green Angiography in Patients with Central Serous Chorioretinopathy. *J Clin Med*. 2021; **10**, 4525 .
24. Zola M, Bousquet E, Favard C, Gigon A, Mantel I, Behar-Cohen F INDOCYANINE GREEN ANGIOGRAPHY OF TYPE 1 MACULAR NEOVASCULARIZATION IN AGE-RELATED MACULAR DEGENERATION AND CENTRAL SEROUS CHORIORETINOPATHY REVEALS DIFFERENT DISEASE MECHANISMS. Retina. 2023 Aug 1;43(8):1255-1263
25. A. Gaudric, S. Mrejen, WHY THE DOTS ARE BLACK ONLY IN THE LATE PHASE OF THE INDOCYANINE GREEN ANGIOGRAPHY IN MULTIPLE EVANESCENT WHITE DOT SYNDROME. *Retin Cases Brief Rep*. 2017; **11 Suppl 1**, S81–S85.
26. N. Pankova, X. Zhao, H. Liang, D. S. H. Baek, H. Wang, S. Boyd, Delayed near-infrared analysis permits visualization of rodent retinal pigment epithelium layer in vivo. *J Biomed Opt*. 2014; **19**, 076007.
27. E. Botos, J. Klumperman, V. Oorschot, B. Igyártó, A. Magyar, M. Oláh, A. L. Kiss, Caveolin-1 is transported to multi-vesicular bodies after albumin-induced endocytosis of caveolae in HepG2 cells. *J Cell Mol Med*. 2008; **12**, 1632–1639.
28. D. Shang, T. Peng, S. Gou, Y. Li, H. Wu, C. Wang, Z. Yang, High Mobility Group Box Protein 1 Boosts Endothelial Albumin Transcytosis through the RAGE/Src/Caveolin-1 Pathway. *Sci Rep*. 2016; **6**, 32180.
29. X. Gu, A. M. Reagan, M. E. McClellan, M. H. Elliott, Caveolins and caveolae in ocular physiology and pathophysiology. *Prog Retin Eye Res*. 2017; **56**, 84–106.
30. E. H. Harrison, Mechanisms of Transport and Delivery of Vitamin A and Carotenoids to the

574 Retinal Pigment Epithelium. *Mol Nutr Food Res*. 2019; **63**, e1801046 .
575 31. N. Tserentsoodol, J. Sztein, M. Campos, N. V. Gordiyenko, R. N. Fariss, J. W. Lee, S. J. Fliesler, I.
576 R. Rodriguez, Uptake of cholesterol by the retina occurs primarily via a low density lipoprotein
577 receptor-mediated process. *Mol Vis*. 2006; **12**, 1306–1318.
578 32. J. O. Kokkonen, P. T. Kovanen, The metabolism of low density lipoproteins by rat serosal mast
579 cells. *Eur Heart J*. 1990; **11 Suppl E**, 134–146.
580 33. J. O. Kokkonen, P. T. Kovanen, Accumulation of low density lipoproteins in stimulated rat
581 serosal mast cells during recovery from degranulation. *J Lipid Res*. 1989; **30**, 1341–1348 .
582 34. E. Bousquet, M. Zhao, B. Thillaye-Goldenberg, V. Lorena, B. Castaneda, M. C. Naud, C. Bergin, B.
583 Besson-Lescure, F. Behar-Cohen, Y. de Kozak, Choroidal mast cells in retinal pathology: a
584 potential target for intervention. *Am. J. Pathol.* 2015; **185**, 2083–2095.
585 35. A. Weerasuriya, G. L. Curran, J. F. Poduslo, Blood-nerve transfer of albumin and its implications
586 for the endoneurial microenvironment. *Brain Res*. 1989; **494**, 114–121.
587 36. M. Mata, J. Staple, D. J. Fink, The distribution of serum albumin in rat peripheral nerve. *J*
588 *Neuropathol Exp Neurol*. 1987; **46**, 485–494.
589 37. H. Koike, S. Ikeda, M. Takahashi, Y. Kawagashira, M. Iijima, Y. Misumi, Y. Ando, S.-I. Ikeda, M.
590 Katsuno, G. Sobue, Schwann cell and endothelial cell damage in transthyretin familial amyloid
591 polyneuropathy. *Neurology*. 2016; **87**, 2220–2229.
592 38. H. Koike, T. Nakamura, R. Nishi, S. Ikeda, Y. Kawagashira, M. Iijima, M. Katsuno, G. Sobue,
593 Widespread Cardiac and Vasomotor Autonomic Dysfunction in Non-Val30Met Hereditary
594 Transthyretin Amyloidosis. *Intern Med*. 2018; **57**, 3365–3370.
595 39. F. Mano, A. Dispenzieri, S. Kusaka, C. Pavesio, H. Khalid, P. A. Keane, J. S. Pulido,
596 ASSOCIATION BETWEEN CHOROIDAL CHARACTERISTICS AND SYSTEMIC SEVERITY IN
597 AMYLOIDOSIS. *Retina*. 2021; **41**, 1037–1046.
598 40. Shiragami C, Shiraga F, Matsuo T, Tsuchida Y, Ohtsuki H. Risk factors for diabetic choroidopathy
599 in patients with diabetic retinopathy. Graefes Arch Clin Exp Ophthalmol Albrecht Von Graefes
600 Arch Klin Exp Ophthalmol. 2002;240(6):436-442.
601 41. Galiero R, Caturano A, Vetrano E, et al. Peripheral Neuropathy in Diabetes Mellitus: Pathogenetic
602 Mechanisms and Diagnostic Options. Int J Mol Sci. 2023;24(4):3554. doi:10.3390/ijms24043554

603